Journal of Catalysis **191,** 332–347 (2000)
doi:10.1006/jcat.1999.2809, available online at http://www.idealibrary.com on IDEAL®

Characterization of Gold–Titania Catalysts via Oxidation of Propylene to Propylene Oxide

Eric E. Stangland, Kevin B. Stavens, Ronald P. Andres, and W. Nicholas Delgass[1]

School of Chemical Engineering, Purdue University, West Lafayette, Indiana 47907-1283

Received July 21, 1999; revised December 23, 1999; accepted December 23, 1999

Propylene oxidation to propylene oxide (PO) was performed with an H_2/O_2 mixture in the temperature range of 373–473 K using Au/TiO_2 catalysts synthesized by a variety of techniques, including one which produced Au–Ti nanoclusters with controlled composition. The two most PO-active catalysts were one prepared by deposition–precipitation of gold onto titania-modified silica and one consisting of silica-supported Au–Ti nanoclusters with a 200 : 1 gold-to-titanium ratio. Most Au/TiO_2 catalysts had a small spread in PO activity and selectivity at 373 K, but gave a much wider distribution in performance at temperatures above 413 K. With very few exceptions, these catalysts exhibit a maximum in PO turnover frequency over the experimental temperature range, resulting from sequential reaction of PO to other oxidation products. The largest observed losses in PO selectivity with increasing temperature and decreasing WHSV were to the oxidative cracking products ethanal and CO_2, suggesting that maximizing the number of PO active sites is not the only solution to increase PO yields over these catalysts. The amount, phase, and method of contacting titania with gold controlled both PO oligomerization, as seen in the time on stream studies, and H_2-assisted oxidative cracking rates. Catalysts that have isolated Ti atoms, such as the silica-supported Au–Ti nanoclusters, generally maintain a higher selectivity to PO with temperature. A D_2 kinetic isotope effect was observed for PO formation which strongly suggests that a hydroperoxy intermediate is involved in the rate-limiting step for PO formation.

Key Words: **propylene; partial oxidation; propylene oxide; gold; titania; nanocluster; epoxidation; kinetic isotope effect.**

1. INTRODUCTION

The low catalytic activity of bulk gold surfaces is related to its inertness toward simple molecules such as H_2, O_2, and CO as illustrated by Hammer and Nørskøv for the case of H_2 using DFT calculations (1). The reactivity of the Au surface, however, is drastically altered when gold is well dispersed on metal oxide support materials. For many catalytic reactions the choice of support, preparation method, and resulting Au particle size can dramatically affect gold reactivity, resulting in enhanced catalytic rates or unique reactivity as compared to those of bulk gold. These effects have been observed for H_2–D_2 (2) and $^{16}O_2$–$^{18}O_2$ exchange reactions (3), hydrogenation and hydrogenolysis (4), hydrochlorination (5), and selective oxidation reactions (6, 7). The last 10 years have seen intensive research on the activity of metal oxide supported gold catalysts, particularly for low-temperature CO oxidation over Au/TiO_2 (8–16). Spectroscopic investigations are beginning to show how the preparation method controls the gold/titania interface, creating active sites for CO and O_2 adsorption and subsequent reaction (17–23).

Recently, Haruta and co-workers have reported that certain Au/TiO_2 catalysts exhibit activity and greater than 90% selectivity for the production of propylene oxide (PO) from propylene, O_2, and H_2 at temperatures between 303–393 K (24–27). Only catalysts in which gold is deposited as particles larger than 2 nm in diameter by deposition–precipitation (DP) onto certain titania support materials such as anatase, titania-modified silica, Ti-MCM-41, or TS-1 exhibit high PO selectivity (26, 28). Gold particles smaller than 2 nm in diameter show a shift in selectivity from PO to propane (24). Recent scanning tunneling microscopy/spectroscopy studies show that gold atoms deposited in low concentrations on TiO_2 (110) form very flat raftlike particles one or two atomic layers in height. A maximum in CO oxidation catalytic activity on these particles has been related to an apparent 0.2–0.6 eV band gap beginning at particles about 3.5 nm in diameter and smaller (20). These observations may explain propane formation over Au/TiO_2, but a direct link to PO formation has not been made. The exact reaction mechanism and active site for PO formation remain unknown, although a hydroperoxy mechanism has been suggested (25, 28).

The discovery of a catalyst that exhibits activity for direct vapor-phase propylene epoxidation or *in situ* peroxy formation from H_2/O_2 would be of tremendous industrial significance. However, despite the potential of the gold–titania system, problems of industrial viability still exist. At temperatures below 393 K, PO selectivities can be greater than 99%, but Nijhuis *et al.* have shown that while PO

[1] To whom correspondence should be addressed. Fax: 765-494-0805. E-mail: delgass@ecn.purdue.edu.

0021-9517/00 $35.00

selectivity is high, maximum PO yields of greater than 2% could not be achieved due to a rate limitation at high PO partial pressures with loss of PO via oligomerization or further surface reactions (28). Attempts to improve the rate of propylene conversion to PO by raising the temperature only resulted in further combustion of the PO product (28) and a decrease in the already unsatisfactory H_2 efficiency (24).

To further probe the origin and pitfalls of the unique epoxidation activity of the Au/TiO_2 system, we prepared and analyzed catalysts by a variety of techniques, including an aerosol method using a distributed arc cluster source (DACS) (29, 30) which produced intimately mixed Au–TiO_2 nanoclusters of controlled compositions which were subsequently supported on SiO_2. The data provides direct kinetic comparisons of PO formation rate and the further oxidation rates for various types of Au/TiO_2 catalysts in an attempt to elucidate the effects of varied gold-titania contacting. The temperature range was extended to 473 K to accentuate chemical effects on PO selectivity in an attempt to further characterize catalyst limitations.

2. CATALYSTS AND METHODS

The preparation methods for the many different types of conventional and DACS catalysts prepared during the course of this study are summarized below. All conventional catalysts were calcined at 673 K, and DACS catalysts at 573 K, using a heating rate of 2 K min^{-1} in a 20% O_2/balance He mixture for 3 h unless otherwise specified. Table 1 includes a list of the catalysts used and their abbreviations. The gold and, in some cases, titanium weight loadings were determined using a Perkin Elmer 3110 atomic absorption (AA) spectrometer on catalyst samples digested in aqua regia/HF solutions. Total surface areas (S_{BET}) were obtained from BET analysis of N_2 adsorption isotherms using a Micromeretics ASAP 2000 surface area analyzer after catalyst outgassing under vacuum at 393 K for a minimum of 2 h. Additionally, all catalyst supports were checked for crystallographic phase by XRD using a Siemens D500 diffractometer employing Cu X rays.

For some preparations, XPS analysis was performed on a Perkin Elmer 5300 series spectrometer [base pressure during analysis, 10^{-9} Torr (1 Torr = 133.3 N m^{-2})] with an Mg anode powered at 300 W and an acceleration voltage of 15 keV. Ejected photoelectrons were selected with a hemispherical monochromator at pass energy of 8.95 eV before reaching a position-sensitive detector. Calibration using a gold foil (Alfa, 99.9999%) set the Au $4f_{7/2}$ photoline binding energy to 83.9 eV. Gold was undetectable by XPS on supported catalysts with Au loadings below 1 wt%. For uncalcined CP or DP catalysts, Au 4*f* BEs ranged from 83.8 to 85.5 eV, showing both metallic and higher binding energy gold states, which collapsed to a single Au 4*f* metallic photoline at 83.9 eV after calcination.

The average gold particle diameter, $\langle D_p \rangle$, was determined by measuring at least 50 particles from TEM (JEOL 2000 FX at 200 keV) micrographs using Optimus Version 6.1 image analysis software. Table 1 presents the gold loading and the postcalcination Au particle size for each catalyst. Postreaction TEM showed that the metal particle size on

TABLE 1

Characterization Results for Gold–Titania Catalysts

Catalyst	Preparation method	Gold loading (wt%)	D_p (nm)	Amount used for activity testing (g)
Au powder		100	~1000	0.12
0.5-T/Au	TTIP on Au powder	99.5	~1000	0.15
3.0-T/Au	TTIP on Au powder	97.0	~1000	0.61
$AuTi_3$-L	Leached $AuTi_3$ alloy	94.0	~1000	0.26
(Au)/P25	DACS Au cluster on P25	1.7	7.6 ± 3.1	0.09
HTC(Au)/P25	(Au)/P25 after HTC	1.7	16.3 ± 10.6	0.09
Au(I)/A	Au impregnation on anatase	0.2	21.0 ± 10.0	0.28
AuTi(CP)	Coprecipitation	1.4	7.4 ± 1.7	1.10
Au(DP)/P25	Au DP on P25	1.1	7.4 ± 2.3	0.12
Au(DP)/A	Au DP on anatase	0.2	4.5 ± 1.0	0.11
Au(DP)/T-S(α)	Au DP on modified-M5	0.5	4.2 ± 1.0	0.12
Au(DP)/T-S(β)	Au DP on modified-M5	1.1	5.4 ± 1.5	0.05
(Au : Ti, 4 : 1)/S	DACS Au–Ti clusters on M5	0.3	11.1 ± 10.0	0.60
(Au : Ti, 42 : 1)/S	DACS Au–Ti clusters on M5	0.3	9.8 ± 6.0	0.47
(Au : Ti, 200 : 1)/S	DACS Au–Ti clusters on M5	0.2	3.0 ± 2.0	0.30
(Au : Ti, 300 : 1)/S	DACS Au–Ti clusters on M5	0.3	3.6 ± 2.0	0.37
(Au : Ti, >300 : 1)/S	DACS Au–Ti clusters on M5	0.6	5.0 ± 2.8	0.44

Note. Abbreviations: titanium tetraisopropoxide, TTIP; distributed arc cluster source, DACS; impregnation, I; coprecipitation, CP; deposition–precipitation, DP; high-temperature calcination, HTC. The ratio in parentheses for the DACS Au–Ti cluster on M5, e.g., (4 : 1), is the Au : Ti ratio as determined by XPS.

any catalyst was not significantly altered during the course of the catalytic studies.

2.1. Conventional Catalyst Preparation

High-purity gold powder (Engelhard, 99.9999%, S_{BET} = 1 m^2/g) was used as a baseline for bulk gold activity. XPS analysis showed that there was about a 6% surface Ag impurity. Impregnating this Au powder with titanium tetraisopropoxide (TTIP) (Aldrich Chemicals, 97.0%) in a pentane solution at room temperature produced TiO_2-modified Au powders (T/Au, S_{BET} = 1 m^2/g) of different TiO_2 loadings after pentane evaporation. These catalysts, prepared from the Au powder, had typical particle sizes in the 1 μm range, although TEM revealed the presence of smaller nanometer-sized particles. These catalyst were calcined at 573 K to minimize particle sintering.

A higher surface area unsupported catalyst ($AuTi_3$-L, S_{BET} = 4 m^2/g) was prepared by using 80 ml of a 2 M HF solution to selectively leach the Ti phase from 1 g of $AuTi_3$ alloy prepared from high-purity gold shot (Alfa, 99.9999%) and titanium wire (Alfa 99.99%) via arc melting in vacuum. The leach time was 40 min, at which time evolution of H_2 had ceased. Selective leaching was confirmed by XRD, where the initial diffraction pattern of a pure $AuTi_3$ alloy changed to broadened diffraction lines corresponding to pure gold. This catalyst was calcined at 473 K in an attempt to preserve the higher powder S_{BET}. XPS showed that for both the original $AuTi_3$-L and calcined TiO_2-modified Au powders the observable Ti was in the 4+ state, indicative of TiO_2 formation. The $AuTi_3$-L catalyst additionally showed that a large amount of residual fluoride ion remained on the catalyst surface. No distinct TiF_4 or associated phase, however, was detected. This residual fluoride may have an adverse effect on catalytic activity.

Impregnated (I) Au/TiO_2 catalysts were prepared by the addition of an $HAuCl_4 \cdot xH_2O$ (Strem Chemicals, 99.9% Au) aqueous solution to the incipient wetness point of Degussa P25 (S_{BET} = 45 m^2/g), anatase (Aldrich, 99.9+%, S_{BET} = 8 m^2/g, Au(I)/A), or SiO_2 (Cab-o-Sil M5, S_{BET} = 240 m^2/g). XRD showed the P25 to be a mixture of a significant rutile phase with the majority anatase, the Aldrich anatase to be pure, and the M5 to be amorphous.

A coprecipitated (AuTi(CP)) catalyst was prepared by mixing the desired amount of an aqueous solution of $HAuCl_4$ with one that contained $TiCl_4$ dissolved in 2 M HCl. A saturated Na_2CO_3 (Aldrich, 99.5%) solution was added dropwise at room temperature, neutralizing the mixture to approximately pH 7. This solution was stirred vigorously and digested for 1 h. The resulting white precipitate was then filtered, washed three times in 100 ml of hot water (approx. 323 K), and calcined at 573 K. The surface area of the coprecipitated catalyst was about 150 m^2/g, but collapsed to about 50 m^2/g after calcination. The as-prepared material exhibited weak, broad anatase XRD lines, which disappeared in favor of small amounts of rutile in a mostly amorphous matrix after calcination.

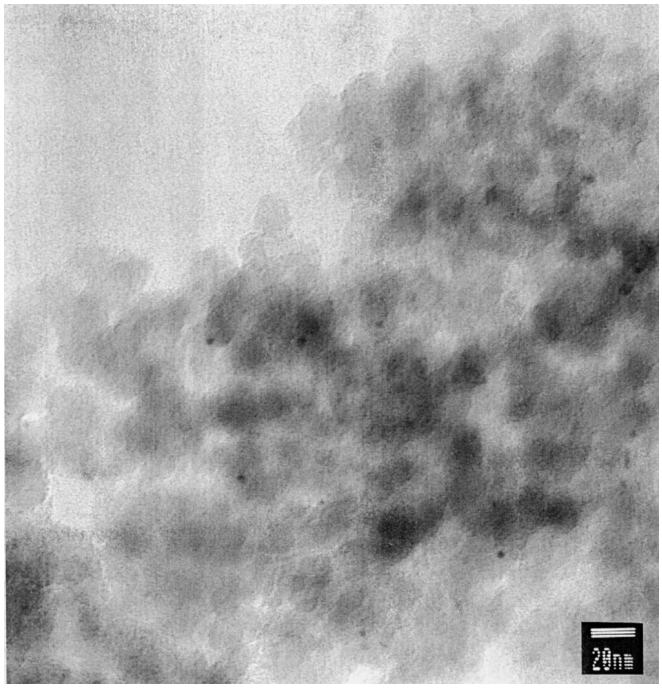

FIG. 1. Transmission electron micrograph of Au(DP)/T-S(α).

Deposition–precipitation (DP) catalysts were prepared by Na_2CO_3 neutralization to pH 7–9 of a room temperature aqueous $HAuCl_4$ solution containing the desired TiO_2 support: either P25 (Au(DP)/P25), anatase (Au(DP)/A), or TiO_2-modified M5 (Au(DP)/T-S). The procedure was similar to that described in Ref. (8). The suspensions were stirred vigorously for 3–4 h before being filtered, washed three times in 100 ml of hot water (approx. 323 K), and calcined at 673 K. Figure 1 shows a TEM micrograph of Au(DP)/T-S(α), while Fig. 2 is a micrograph of Au(DP)/A. These micrographs were typical for catalysts in this study.

The TiO_2-modified M5 support (T-S) was prepared by impregnation of the M5 support with TTIP in pentane, which then evaporated. The resulting solid was calcined at 773 K prior to Au DP. The T-S support had an S_{BET} after calcination of 220 m^2/g. The Ti : Si atomic ratio for the T-S support as determined by XPS was 0.12, which is in good agreement for well-dispersed systems of this TiO_2 weight loading and initial SiO_2 surface area (31). Since no TiO_2 XRD signal was observed, the TiO_2 overlayer on the T-S was either amorphous or existed as very small crystalline domains.

2.2. DACS Catalyst Preparation

The distributed arc cluster source (DACS) is a gas-phase flow reactor which produces single component and multicomponent metal particles with diameters in the nanometer size range (29, 30). As shown in Fig. 3, a negatively biased tungsten rod is brought into close proximity with a

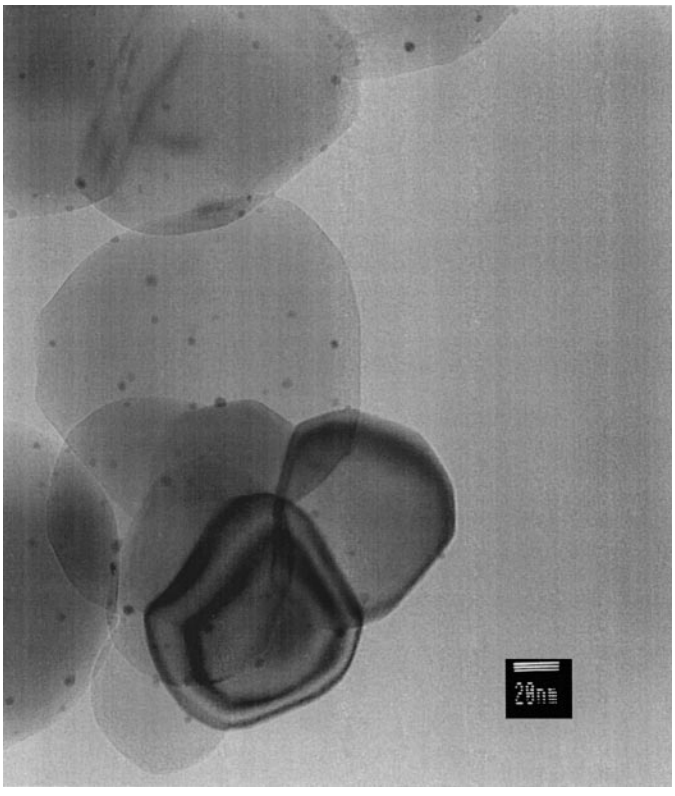

FIG. 2. Transmission electron micrograph of Au(DP)/A.

positively biased carbon crucible containing Au or an Au/Ti mixture to initiate an argon ion plasma. At arc initiation, the sample temperature rises to a point where a substantial metal vapor pressure is established inside the crucible and the argon ion plasma develops into a metal ion plasma and forms a distributed arc serving as the energy source that vaporizes the metal. The hot metal vapor diffuses out of the arc region where it is rapidly mixed with cooler argon gas, creating a supersaturated vapor which then condenses. The growing metal clusters are swept away by the cool carrier gas. The cluster aerosol is further cooled and diluted by a room temperature quench gas, typically helium, to limit cluster–cluster aggregation while the clusters are transported to a capture vessel. The composition of the metal mixture placed in the carbon crucible controls the composition of the multicomponent clusters.

Clusters were captured either as a sol or by depositing them onto a catalytic support material. To generate a stable sol, the nanoclusters were scrubbed from the aerosol into mesitylene (Aldrich, 97%) containing a dodecanethiol surfactant which adsorbed on the surface of the clusters preventing aggregation, resulting in a stable colloid that could be worked up for further analysis. To make a catalyst, the clusters were scrubbed with a slurry of the desired support material in mesitylene without surface-active agents; this resulting material was filtered from the solvent, dried, and calcined at 573 K. DACS catalysts were produced using high-purity titanium wire (Alfa, 99.99%) and/or gold shot (Alfa, 99.9999%). Catalyst (Au)/P25 was generated from nanometer-sized DACS gold particles deposited onto P25. Five DACS Au-TiO_2/SiO_2 catalysts, (Au : Ti)/S, of varied Au : Ti ratio were produced from bimetallic clusters captured onto SiO_2 (Cab-o-Sil, M5). Figure 4 shows a micrograph of the typical DACS bimetallic cluster

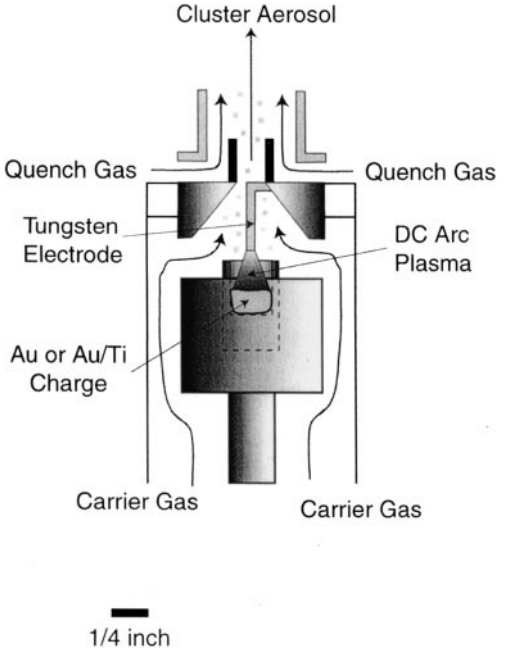

FIG. 3. Distributed arc cluster source (DACS) internal schematic.

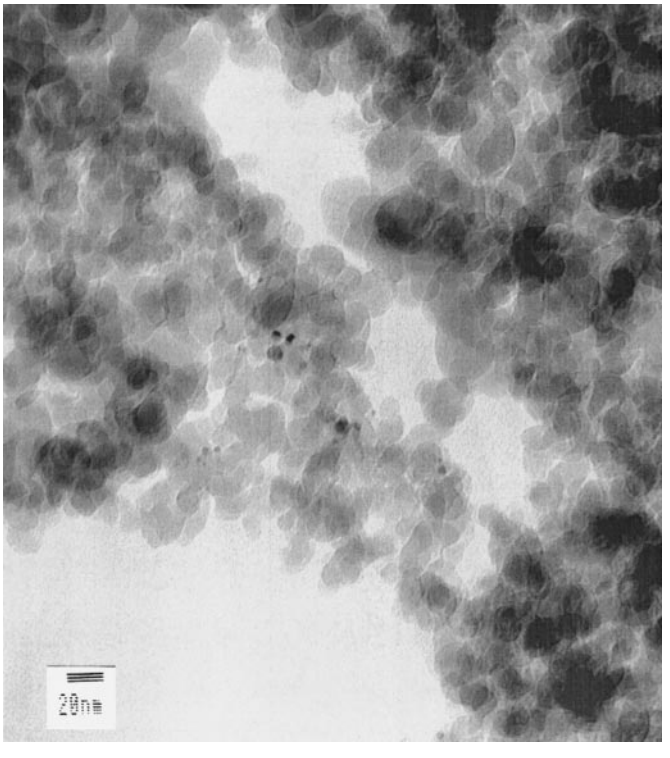

FIG. 4. Transmission electron micrograph of (Au : Ti, 200 : 1)/S.

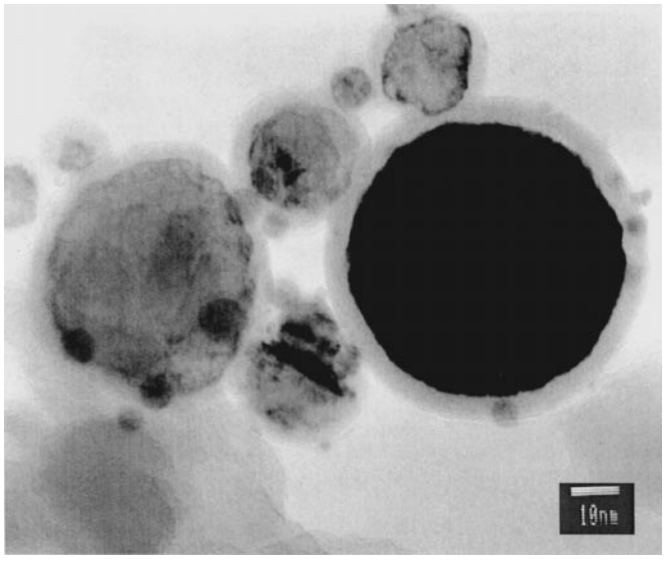

FIG. 5. Transmission electron micrograph of (Au : Ti, 4 : 1)/S showing Au and TiO_2 phase segregation.

catalyst, (Au : Ti, 200 : 1)/S. Specific information is tabulated in Table 1, where it is shown that the DACS clusters tend to have a wider particle size distribution due to the aerosol production method as compared to DP catalysts.

The Ti metal loading of the (Au : Ti, 200 : 1)/S and larger Au : Ti ratio catalysts was too low for AA compositional analysis, so XPS was used for determining the relative Au : Ti ratios between clusters. Surfactant-stabilized Au–Ti cluster sols were prepared in parallel with catalyst preparation, and it was assumed that this sol was representative of the clusters deposited on SiO_2. After removal of excess surfactant, the cluster sol was cast into monolayer films on silver foil (32) and the XPS relative peak areas were determined and corrected for photoionization cross sections (33) and electron escape depth corrections (34) in a homogeneous model. It was assumed that due to the small cluster size, and the monolayer coverage of the Au–Ti clusters on the Ag foil, the XPS atomic ratios were representative of the bulk, although this assumption is an increasingly poor one as particles increase in size from 1 nm in diameter. One DACS catalyst, (Au : Ti, >300 : 1)/S, did not show detectable amounts of Ti, and so it was assumed that the Au : Ti ratio was larger than that of the 300 : 1 sample where Ti was observed. XPS shows that the titanium existed as the Ti^{4+} species of TiO_2 at a BE of 459.0 eV before and after calcination. Rapid surface segregation and oxidation of the Ti phase in the DACS Au–Ti clusters (as well as the $AuTi_3$ alloy used for leaching) are expected on the basis of surface free energy arguments and other XPS results (35). This is clearly demonstrated from the micrograph for the DACS catalyst, (Au : Ti, 4 : 1)/S, in Fig. 5, which shows a high-contrast gold core surrounded by a moiety of lighter contrast presumed to be the segregated TiO_2 phase. The presence of some high binding energy Au 4*f* states was observed for the (Au : Ti, 4 : 1)/S and (Au : Ti, 42 : 1)/S. Similar results were seen for the unleached $AuTi_3$ alloy used to produce the $AuTi_3$-L catalyst. What implications these states have for propylene epoxidation are still unknown, and Au chemical shift interpretation must be reserved until the final state effects are fully evaluated since the BE shift is a combination of both final and oxidation state contributions (36).

2.3. Kinetic Analysis

Kinetic measurements were obtained using a 1/2-in.-diameter stainless steel reactor with a catalyst charge packed between two glass wool plugs. Table 1 gives the amounts of each catalyst used. A thermocouple used to control reactor temperature passed through the catalyst bed from the bottom, and rested at the top edge of the charge. All catalyst samples were pretreated at 573 K in 20% O_2 (99.999%), balance He (99.995%) at 50 STP cc min^{-1} for 3 h prior to catalytic activity assessment, except for the leached $AuTi_3$ alloy which was pretreated at 473 K. Reactant concentrations used for the propylene oxidation experiments were 10/10/10/70 vol% of propylene (99.9%), O_2, H_2 (99.9995%), and He, respectively. In some experiments, D_2 (99.99%) was substituted for H_2. All gases were used without further purification. PO and acrolein oxidation experiments were performed by entraining the relevant oxygenate in a gas mixture of 10/10/80% H_2/O_2/He by passing it through a sealed gas/liquid saturator kept at the temperature of a dry ice/isopropanol slurry, approximately 200 K. Precautions are warranted as all reactant mixtures are inside the flammability envelope.

An activity experiment consisted of a temperature program of 473–413–433–373 K, holding for 6 h at each temperature and taking samples at 35-min. intervals. After this program, the 473 K temperature was immediately retested for approximately 3 h. Figure 6 shows the time on stream behavior for typical catalysts. In most cases, plots of the

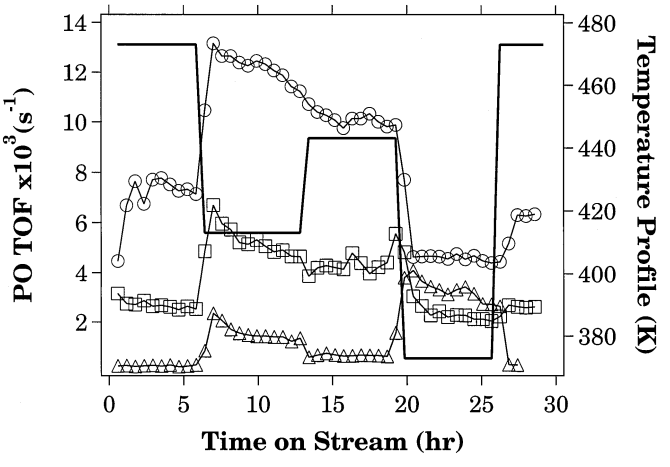

FIG. 6. TOF vs time on stream during the temperature profile for selected catalysts. (○) Au(DP)/T-S(α), (□) (Au : Ti, 200 : 1)/S, (△) Au(DP)/P25, (—) temperature profile.

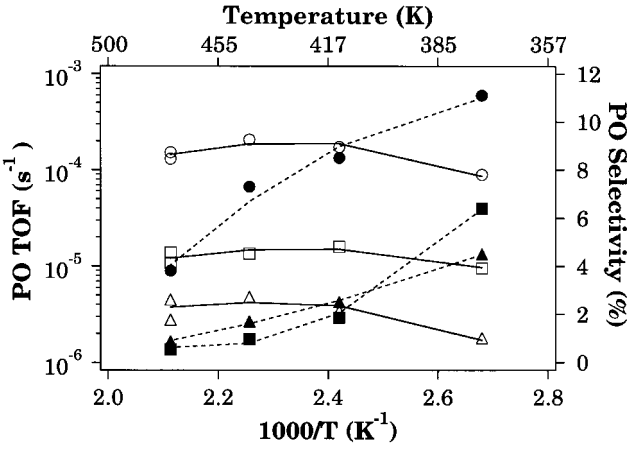

FIG. 7. PO activity and selectivity over TiO_2-modified gold powder catalysts. Reaction conditions were $C_3H_6/O_2/H_2/He = 10/10/10/70\%$ at 35 STP cc min^{-1}. TOF: (○) 0.5-T/Au, (□) 3.0-T/Au, (△) $AuTi_3$-L. Selectivity: (●) 0.5-T/Au, (■) 3.0-T/Au, (▲) $AuTi_3$-L.

TOF data for each catalyst show only minor deactivation between the initial and final 473 K tests (e.g., Figs. 6 and 7). Deactivation is the smallest at 473 K. While as much as 50% of the initial activity can be lost in the first hour for the more unselective catalysts, the activity loss is usually less dramatic for the most active DP and DACS catalysts. In this paper, the reported TOF values represent an average of the last three data points in the given temperature window; the PO activity appeared to have reached the pseudo steady state for most catalysts in this region.

Effluent samples from the reactor were analyzed by a Varian 3740 gas chromatograph using He carrier gas, a Chromosorb 102 packed column (Supelco, Inc.) with a TCD detector to monitor H_2, O_2, CH_4, CO_2, propylene, and propane, and a Supelcowax 10 capillary column (Supelco, Inc.) with an FID detector to monitor ethanal, propylene oxide, propanal, acetone, acrolein, and traces of other oxygenates. The He carrier gas maximizes TCD sensitivity and detection of trace components. The nonlinearity of the H_2/He mixture thermoconductivity, however, made it impossible to quantify the H_2 conversion in this phase of the study. Despite the undetermined linearity of the D_2/He mixture, we were able to estimate D_2 conversions and thus the D_2 efficiency for some of the catalysts. TCD sensitivity was about 100 ppm for the reactants and products while the FID sensitivity to the oxygenates was about 100 ppb.

Turnover frequencies (TOFs) were calculated on the basis of the determination of the apparent gold particle surface area using $\langle D_p \rangle$ and the AA results for the Au weight loading. A hemispherical particle model and an Au metal density of 19.3 g cm^{-1} were assumed. For gold powder catalysts, we used the BET surface area for TOF normalization. Since the active sites are most likely at the Au–Ti interface, rate normalization to Au surface area provides a lower bound to the TOF, giving a quantitative comparison between catalysts of the fraction of active gold atoms. TOFs were used to calculate selectivity to product i defined as $\nu_i(\mathrm{TOF}_i)/\sum \nu_k(\mathrm{TOF}_k)$, where the denominator is the sum of TOFs for the k oxidation products observed and ν is the appropriate stoichiometric coefficient. In cases where the selectivity does not add up to 100%, the difference was made up by small amounts of CH_4, usually found only at temperatures above 443 K.

3. RESULTS

3.1. Activity of Au Powders

To determine the importance of Au–Ti contacts, we first added Ti directly to gold in the absence of a support. A kinetic summary of propylene oxidation at 413 K over gold and modified gold powders is shown in Table 2. Figure 7

TABLE 2

Kinetic Results for Propylene Oxidation over TiO_2-Modified-Gold Powders at 413 K

	Au powder		0.5-T/Au		3.0-T/Au		$AuTi_3$-L	
Species	TOF ($\times 10^3$ s^{-1})	Sel. (%)	TOF ($\times 10^3$ s^{-1})	Sel. (%)	TOF ($\times 10^3$ s^{-1})	Sel. (%)	TOF ($\times 10^3$ s^{-1})	Sel. (%)
Propylene	2.11	0.13[a]	2.03	0.16[a]	0.85	0.29[a]	0.14	0.11[a]
Oxygen	0.005	0.0004[b]	0.64	0.08[b]	0.27	0.14[b]	0.18	0.22[b]
Ethanal			0.04	1.4	0.04	3.0	0.01	6.0
PO			0.17	8.5	0.02	1.9	0.003	2.5
Acetone	0.01	0.5	0.004	0.2	0.004	0.4	0.001	1.1
Propanal			0.09	4.3	0.06	7.3	0.04	29.3
Acrolein							0.001	0.7
CO_2			0.32	5.3	0.14	5.5	0.10	24.9
Propane	2.10	99.5	1.60	80.2	0.70	81.9	0.05	35.6

Note. Reaction conditions were $C_3H_6/O_2/H_2/He = 10/10/10/70\%$ at 35 STP cc min^{-1}.

[a] Conversion of propylene in %.

[b] Conversion of oxygen in %.

shows the PO formation TOF and selectivity over the entire temperature range investigated.

Bulk Au powder exhibited significant hydrogenation activity, producing mostly propane with small amounts of acetone for the temperatures studied. When gold/titania interfaces were created, however, either by treating Au powder with TTIP or by leaching $AuTi_3$, the resulting materials exhibited activity to PO and other oxygenates in addition to slightly reduced propane formation. The observed oxygenates were the same as those observed by Nijhuis *et al.* (28), and appeared in all experiments reported here. The catalyst with 10 theoretical monolayers of TiO_2, 0.5-Ti/Au, had the highest levels of PO activity, while that with 60 monolayers of TTIP, 3.0-T/Au, resulted in an activity decrease for all oxygenates and propane. A higher Ti loaded but possibly fluoride poisoned material, $AuTi_3$-L, exhibited the lowest activity to oxygenates and propane. Since bulk P25 only exhibited hydrogenation activity to propane with a TOF of 3.1×10^{-4} and CO_2 formation with a TOF of 1.4×10^{-5} at 413 K, based on the P25 BET surface area, the Au–Ti interface is the likely location of the partial oxidation sites.

3.2. *Activity of Supported Catalysts*

Most supported catalysts typically showed a maximum in PO TOF at temperatures between 413 and 473 K, while for certain catalysts this maximum was below 373 K. Both the Mears criterion for the absence of external diffusion and the Wiesz–Prater criterion for the absence of internal diffusion were satisfied in this work, suggesting that the maximum does not originate from transport effects (37). Higher temperatures resulted in varied but generally large increases in ethanal and CO_2 selectivities at the expense of PO formation. The following sections describe the PO formation rate and selectivity for a series of catalysts for which the preparation method was designed to increase the intimacy of Au–Ti contacting. Figures 8 and 9 collectively plot PO TOF and selectivity for the non-DACS bimetallic catalysts, except for the (Au : Ti, 200 : 1)/S catalyst, which is shown for comparison.

3.2.1. Improved contacting vs modified-Au powders. Improved Au–Ti contacting (i.e., a greater number of Au–Ti interface sites) compared to that of TiO_2-modified gold powders was accomplished by supporting small gold particles on anatase by impregnation or on P25 using DACS Au nanoclusters. A summary of the kinetics at 413 K for these catalysts can be found in Table 3.

Although Figs. 8 and 9 show a fairly high PO TOF and selectivity for Au(I)/A, its propylene conversion and PO yield were the poorest of any catalyst, including those created by Au powder modification. This material would be uninteresting except for the fact that Hayashi *et al.* have reported that impregnated catalysts do not produce PO. In their studies, however, an anatase Nippon aerosil P25 support of much higher surface area was used (25). Attempts in our laboratory to create active impregnated Degussa P25 or pure rutile catalysts also failed. Despite the large $\langle D_p \rangle$ observed for Au(I)/A, Shastri *et al.* have described situations in which anatase impregnation catalysts can have a bimodal Au particle size, with some very large particles and some small highly dispersed particles (38). Although our TEM resolution was not good enough to detect these particles in Au(I)/A, they may exist as the actual PO active sites.

When gold was impregnated onto anatase via chloroauric acid, it began as an oxidized species that, upon calcination, quickly sintered to large metallic particles. Colloidal approaches to Au particle deposition have succeeded in

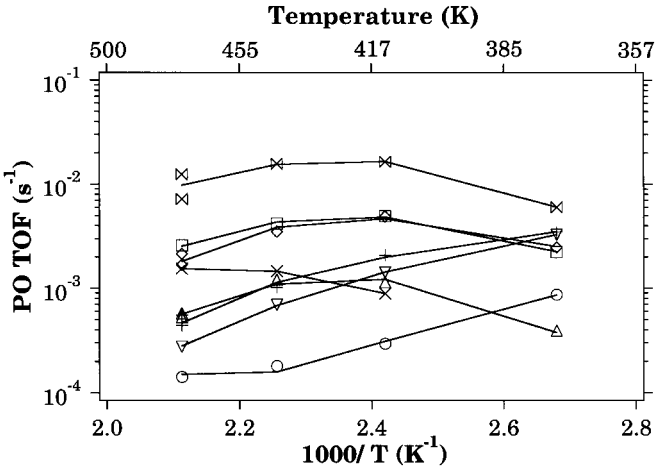

FIG. 8. PO activity of titania-supported gold catalysts. Reaction conditions were $C_3H_6/O_2/H_2/He = 10/10/10/70\%$ at 35 STP cc min^{-1}. TOF: (⋈) Au(DP)/T-S(α), (□) (Au : Ti, 200 : 1)/S, (◇) Au(DP)/A, (×) Au(I)/A, (△) AuTi(CP), (+) HTC(Au)/P25, (▽) Au(DP)/P25, (○) (Au)/P25.

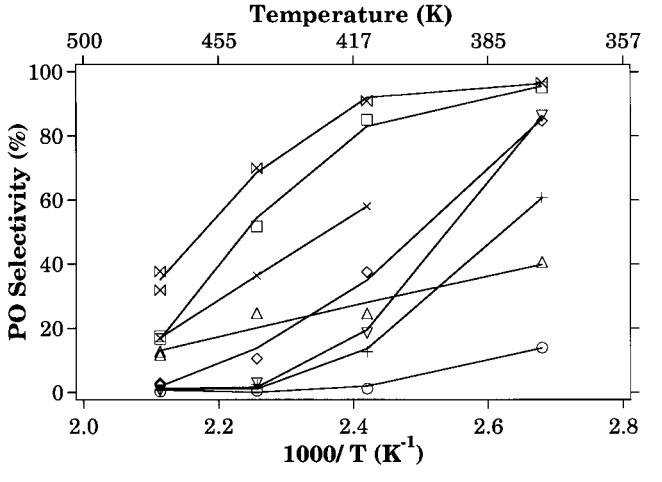

FIG. 9. PO selectivity of titania-supported gold catalysts. Reaction conditions were $C_3H_6/O_2/H_2/He = 10/10/10/70\%$ at 35 STP cc min^{-1}. Selectivity: (⋈) Au(DP)/T-S(α), (□) (Au : Ti, 200 : 1)/S, (◇) Au(DP)/A, (×) Au(I)/A, (△) AuTi(CP), (+) HTC(Au)/P25, (▽) Au(DP)/P25, (○) (Au)/P25.

TABLE 3

Kinetic Results for Propylene Oxidation over Impregnated, DACS Au on TiO_2, and the Coprecipitated Catalyst at 413 K

	Au(I)/A		(Au)/P25		HTC(Au)/P25		AuTi(CP)	
Species	TOF ($\times 10^3$ s^{-1})	Sel. (%)	TOF ($\times 10^3$ s^{-1})	Sel. (%)	TOF ($\times 10^3$ s^{-1})	Sel. (%)	TOF ($\times 10^3$ s^{-1})	Sel. (%)
Propylene	1.5	0.01[a]	2.4	0.95[a]	7.4	0.30[a]	4.6	1.5[a]
Oxygen	3.4	0.03[b]	8.7	0.57[b]	6.9	0.45[b]	2.3	1.3[b]
Ethanal			3.0	8.1	2.2	19.7	0.01	0.1
PO	0.9	58.0	0.3	1.2	0.9	12.7	1.1	24.6
Acetone			0.8	3.2	1.0	13.1		
Propanal			0.2	0.7	0.1	1.1	0.06	1.2
Acrolein								
CO_2	1.9	42.0	4.4	6.1	3.2	14.4	1.1	8.0
Propane			19.3	80.1	2.9	39.0	3.0	66.1

Note. Reaction conditions were $C_3H_6/O_2/H_2/He = 10/10/10/70\%$ at 35 STP cc min^{-1}.
[a] Conversion of propylene in %.
[b] Conversion of oxygen in %.

creating more highly dispersed systems that have some resistance to sintering, while increasing Au–Ti interface sites (16). We achieved a similar effect by depositing nanometer-sized Au clusters from the DACS onto P25 ((Au)/P25) which, despite resulting in a lower PO TOF and selectivity compared to those of Au(I)/A, produced significantly higher specific PO yields. The selectivity to propane over (Au)/P25 was quite high. The particle size distribution suggests that, although the $\langle D_p \rangle$ is around 8 nm, there was a fair number of particles not observed below 2 nm in size which are known to produce propane under these conditions (25).

A high-temperature calcination (HTC) pretreatment at 873 K of (Au)/P25 decreased propane activity by partial Au sintering, increasing the $\langle D_p \rangle$ from 7.6 to 16.3 nm. Figures 8 and 9 show, however, that substantial increases in the PO formation TOF and selectivity occurred for HTC(Au)/P25 despite this increase in particle size. Table 3 shows that after HTC, the formation of other non-PO oxygenates also increased, while the total conversion of propylene decreased. The small amount of sample recovered precluded experiments to detect if a change in the TiO_2 support phase occurred that could account for these reactivity differences. Tsubota *et al.* have ascribed increased CO oxidation activity for gold colloids supported on TiO_2 calcined at higher temperature to the formation of stronger interactions between the gold and titania phases (15).

An AuTi(CP) catalyst was prepared in an attempt to further increase gold–titania interfacial contact through intimate mixing at the preparation step prior to calcination. Figure 9 and Table 3 indicate that this catalyst was more PO selective over the temperature range studied as compared to the modified powder, impregnated, or (Au)/P25 materials. This catalyst, despite normal online stability, deactivated during storage at ambient conditions, resulting in the loss of all relevant catalytic activity. The specific reason for deactivation is not known, but it may be related to small morphological changes in the gold–titania interface due to prolonged water vapor and oxygen exposure. Small changes in iron phase structure in CP Au/Fe_2O_3 catalysts for low-temperature CO oxidation also result in large activity variation, and it is possible that our preparation method did not yield the most active and stable CP catalyst (39).

3.2.2. Deposition–precipitation onto titania supports. The deposition–precipitation (DP) method has been shown to consistently produce the most active and selective gold–titania catalysts for propylene epoxidation (26, 28). To assess the effects of this preparation method utilizing various titania support materials for comparison to the other catalysts in this study, a series of DP catalysts was prepared on pure anatase (A), Degussa P25, and titania-modified silica (T-S). The data for PO activity and selectivity are found in Figs. 8 and 9, while data for the product distribution at 413 K can be found in Table 4. Table 5 gives product distribution results at 473 K for the A- and T-S-supported materials. The activity and selectivity results reported here for both the Au(DP)/T-S(α) and the Au(DP)/P25 material are very similar for those reported by Nijhuis *et al.* when compared at 373 K (28).

Despite the similar preparation methods, the three DP catalysts showed a wide range of activity and selectivity at temperatures higher than 373 K. Figures 8 and 9 clearly indicate that Au(DP)/T-S(α), the most active material in this study, was more active and selective than Au(DP)/A, which was in turn superior to Au(DP)/P25. While both Au(DP)/T-S(α) and Au(DP)/A clearly showed a rate maximum between 373–473 K, it occurred between 323–373 K (not shown) for Au(DP)/P25, similar to that of the (Au)/P25 catalyst. A similar rate but higher selectivity was observed for Au(DP)/P25 as compared to HTC(Au)/P25. No propane

TABLE 4

Kinetic Results for Propylene Oxidation over DP Catalysts at 413 K

	Au(DP)/T-S(α)		Au(DP)/A		Au(DP)/P25	
Species	TOF ($\times 10^3$ s^{-1})	Sel. (%)	TOF ($\times 10^3$ s^{-1})	Sel. (%)	TOF ($\times 10^3$ s^{-1})	Sel. (%)
Propylene	18.1	0.42[a]	13.0	0.90[a]	7.7	0.03[a]
Oxygen	11.5	0.39[b]	20.2	0.22[b]	14.3	0.77[b]
Ethanal	12.0	4.4	7.0	36.0	4.2	36.2
PO	16.4	90.8	4.9	37.8	1.4	18.6
Acetone	0.1	0.7	0.1	0.5	0.6	7.8
Propanal	0.1	0.5	0.2	1.2	0.1	1.2
Acrolein	0.1	0.4	0.1	0.7		
CO_2	1.7	3.2	9.4	24.0	7.5	32.3
Propane						

Note. Reaction conditions were $C_3H_6/O_2/H_2/He = 10/10/10/70\%$ at 35 STP cc min^{-1}.

[a] Conversion of propylene in %.

[b] Conversion of oxygen in %.

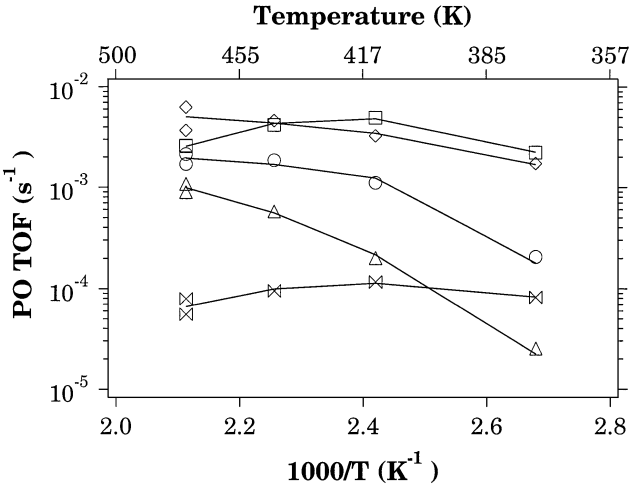

FIG. 10. PO activity of supported DACS (Au : Ti)/S catalysts. Reaction conditions were $C_3H_6/O_2/H_2/He = 10/10/10/70\%$ at 35 STP cc min^{-1}. TOF: (□) (Au : Ti, 200 : 1)/S, (◇) (Au : Ti, 300 : 1)/S, (○) (Au : Ti, 42 : 1)/S, (△) (Au : Ti, >300 : 1)/S, (⋈) (Au : Ti, 4 : 1)/S.

was observed for any DP catalyst, demonstrating the ability of the DP method at a given pH to produce tight Au size distribution (7).

Figure 9 shows that despite similar PO selectivity at 373 K for all the DP catalysts, the selectivity for Au(DP)/T-S(α) decreased in a slower convex manner with increasing temperature, while the selectivity for the other two DP catalysts decreased much more quickly in a concave fashion. Over Au(DP)/A, selectivity to ethanal quickly increased at temperatures above 373 K, while the Au(DP)/P25 catalyst showed slightly more total combustion in the same temperature range, consistent with published reports that DP Au on pure rutile results in catalysts that have high combustion selectivity even at low temperatures (26). It is interesting to note the dramatic effect that small changes in titania phase have on the overall PO activity and selectivity both here and in the work of Haruta *et al.* (26).

3.2.3. DACS bimetallic Au–Ti catalysts. Nijhuis *et al.* have already demonstrated that the problems of PO oligomerization and loss of yield due to bulk extended titania phases are reduced by using gold deposited on a well-dispersed Ti phase (28). In this work, we have attempted to further control Au–Ti intermixing by using the DACS to create bimetallic Au–Ti nanoclusters of various compositions in order to directly assess the effects of Ti dispersion within a gold matrix on PO activity. This cannot be done by normal solution catalyst preparation methods. Figures 10 and 11 show the PO activity and selectivity, respectively, for the five DACS (Au : Ti)/S catalysts prepared

TABLE 5

Kinetic Results for Propylene Oxidation over Selected Catalysts at 473 K

	Au(DP)/T-S(α)		Au(DP)/A		(Au : Ti, 200 : 1)/S		(Au : Ti, 300 : 1)/S	
Species	TOF ($\times 10^3$ s^{-1})	Sel. (%)	TOF ($\times 10^3$ s^{-1})	Sel. (%)	TOF ($\times 10^3$ s^{-1})	Sel. (%)	TOF ($\times 10^3$ s^{-1})	Sel. (%)
Propylene	34.3	0.79[a]	75.1	0.50[a]	16.8	0.38[a]	3.2	0.30[a]
Oxygen	40.3	1.4[b]	143.1	1.5[b]	16.6	0.59[b]	4.1	0.64[b]
Ethanal	17.8	34.7	65.5	58.1	7.8	29.7	0.3	7.6
PO	12.4	36.2	2.2	2.9	2.6	15.3	1.1	33.4
Acetone	2.3	6.7	1.1	1.4	4.0	23.6	0.04	1.3
Propanal	0.8	2.3	1.5	2.0	1.0	5.8	0.8	25.0
Acrolein	0.5	1.4	1.4	1.9	1.2	7.1	0.4	12.0
CO_2	15.3	14.6	71.5	31.7	5.4	10.6	1.9	19.2
Propane			0.6	0.8				

Note. Reaction conditions were $C_3H_6/O_2/H_2/He = 10/10/10/70\%$ at 35 STP cc min^{-1}.

[a] Conversion of propylene in %.

[b] Conversion of oxygen in %.

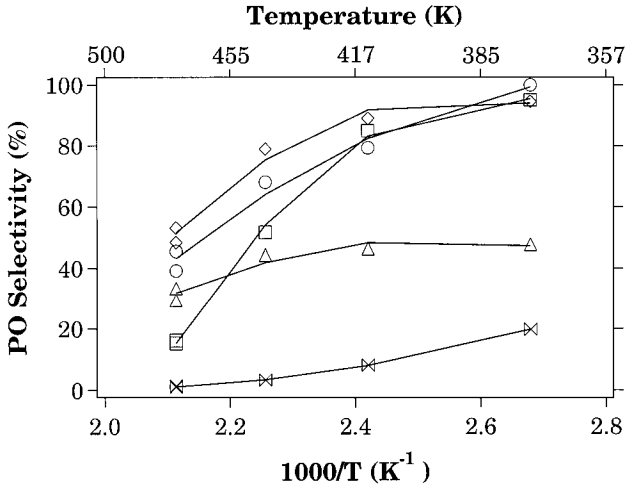

FIG. 11. PO selectivity of supported DACS (Au : Ti)/S catalysts. Reaction conditions were $C_3H_6/O_2/H_2/He = 10/10/10/70\%$ at 35 STP cc min^{-1}. Selectivity: (□) (Au : Ti, 200 : 1)/S, (◇) (Au : Ti, 300 : 1)/S, (○) (Au : Ti, 42 : 1)/S, (△) (Au : Ti, >300 : 1)/S, (⋈) (Au : Ti, 4 : 1)/S.

with different Au : Ti ratios while additional kinetic data at 413 K are found in Table 6. Kinetic data at 473 K for selected bimetallic catalysts can be found in Table 5.

As shown in Fig. 10, at 413 K and below, a clear maximum in PO activity was observed at an Au : Ti ratio of about 200 : 1. At one composition extreme, the (Au : Ti, >300 : 1)/S catalyst had a low TOF due to the small amount of Ti and therefore a low number of active sites associated with the bimetallic clusters. At the other extreme, the (Au : Ti, 4 : 1)/S catalyst had bimetallic clusters, as shown in Fig. 5, with the gold surface largely covered with a TiO_2 phase, resulting in lower PO activity similar to that for the overpromoted gold powder.

Interestingly, at the three intermediate Au : Ti ratios, the DACS clusters all have very high activity and above 80% selectivity at 373 K despite a wide range in cluster composition. Comparison of Figs. 9 and 11 demonstrates that the selectivity to PO for a majority of the DACS catalysts, with the exception of (Au : Ti, 4 : 1)/S, was larger than that for most of the other supported catalysts at every temperature above 413 K. The comparison of the higher temperature activities and selectivities in Table 5 between both the DACS Au–Ti nanoclusters and the best DP catalysts indicated that the well-dispersed DACS Ti limited the formation of ethanal and CO_2, products which tended to dominate the selectivity of most catalysts at temperatures above 413 K. To strengthen this argument, the catalyst with the largest bulk TiO_2 phase, (Au : Ti, 4 : 1)/S, had the highest rate to ethanal of all the DACS bimetallic catalysts. The catalysts with the lowest amount of TiO_2 phase, (Au : Ti, >300 : 1)/S, did not have a maximum in PO activity between 373 and 473 K and had only a slight decrease in PO selectivity with temperature.

Just as was the case for the (Au)/P25 catalysts, the arc source has the possibility of forming small propane-producing Au particles. As shown in Table 6, the 4 : 1, 42 : 1, and >300 : 1 nanoclusters produce propane despite having $\langle D_p \rangle$ greater than 2 nm. It is possible that the higher arc powers necessary to produce the lower Au : Ti ratio clusters produced small stray Au particles not associated with any titanium. The small amount of Ti associated with the >300 : 1 catalysts probably ensures some small propane-producing particles. A monometallic DACS Au catalyst, Au/SiO_2, with a particle size of 4.0 ± 1.4 nm, prepared as a control, had Au particles below 2 nm in size and exhibited a propane TOF 1 order of magnitude higher than those observed for the (Au : Ti)/S catalysts. The (Au : Ti, 200 : 1)/S and (Au : Ti, 300 : 1)/S catalysts did not produce detectable

TABLE 6

Kinetic Results for Propylene Oxidation over DACS (Au : Ti)/S Catalysts at 413 K Listed by Atomic Ratio

	(4 : 1)		(42 : 1)		(200 : 1)		(300 : 1)		(>300 : 1)	
Species	TOF ($\times 10^3$ s^{-1})	Sel. (%)	TOF ($\times 10^3$ s^{-1})	Sel. (%)	TOF ($\times 10^3$ s^{-1})	Sel. (%)	TOF ($\times 10^3$ s^{-1})	Sel. (%)	TOF ($\times 10^3$ s^{-1})	Sel. (%)
Propylene	1.4	0.06[a]	1.4	0.06[a]	5.8	0.1[a]	3.7	0.35[a]	0.4	0.04[a]
Oxygen	1.1	0.08[b]	0.6	0.04[b]	3.5	0.12[b]	2.3	0.35[b]	0.6	0.09[b]
Ethanal	0.2	9.3			0.4	4.5	0.1	2.5	0.05	7.1
PO	0.1	8.2	1.1	79.2	4.9	85.0	3.3	89.0	0.2	46.4
Acetone	0.03	2.1	0.01	0.6	0.2	3.3	0.04	1.2	0.01	0.7
Propanal	0.1	9.5	0.1	4.6	0.2	2.6	0.1	2.0	0.1	20.4
Acrolein	0.01	0.8	0.03	1.8	0.1	2.3	0.1	2.9	0.01	2.1
CO_2	0.6	14.1			0.4	2.4	0.4	3.3	0.3	19.2
Propane	0.7	49.4	0.2	13.4					0.01	3.2

Note. Reaction conditions were $C_3H_6/O_2/H_2/He = 10/10/10/70\%$ at 35 STP cc min^{-1}.

[a] Conversion of propylene in %.

[b] Conversion of oxygen in %.

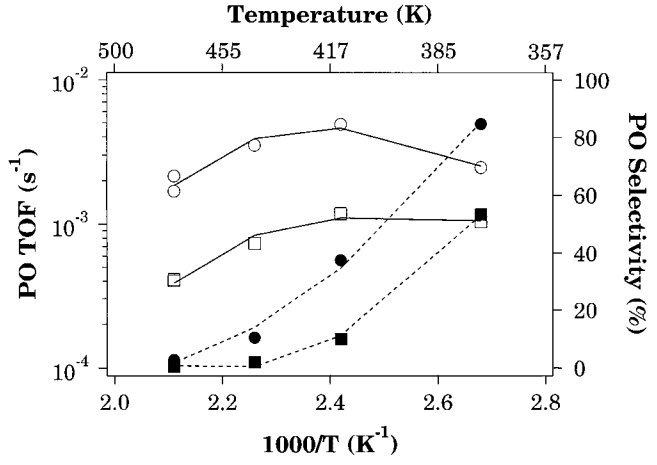

FIG. 12. Effect of propylene conversion on PO selectivity for the Au(DP)/A catalyst. Reaction conditions were $C_3H_6/O_2/H_2/He = 10/10/10/70\%$ at 35 STP cc min^{-1}. Small charge, 0.11 g (at 473 K, O_2 conversion 1.4%, C_3H_6 conversion 0.5%): (○) TOF, (●) selectivity. Large charge, 0.57 g (at 473 K, O_2 conversion 7.8%, C_3H_6 conversion 2.4%): (□) TOF, (■) selectivity.

amounts of propane despite having $\langle D_p \rangle$ around 3.5 ± 2.0 nm. This is reconcilable considering that the standard deviation around the mean was high due to the existence of some much larger particles.

3.3. Conversion Effects on PO TOF and Selectivity

Figure 12 shows the effects of decreasing the weight-hourly-space-velocity (WHSV) for Au(DP)/A. Increasing the catalyst charge from 0.11 to 0.57 g for Au(DP)/A resulted in a 30% decrease in PO selectivity at 413 K. Over the entire temperature range studied, for every decrease in PO selectivity there is a corresponding increase in ethanal selectivity. There was little change in the PO yield for the Au(DP)/A catalyst with decreasing WHSV at temperatures above 443 K due to the intrinsic low selectivity. PO yields at the lower temperatures, however, were slightly enhanced at lower WHSV despite a loss in PO selectivity. The selectivities to other oxygenates showed only small perturbations with WHSV. The results for (Au)/P25 were similar.

A different trend with decreasing WHSV was noticed for the more PO-selective Au(DP)/T-S(α) and (Au : Ti, 200 : 1)/S catalysts. A small increase in conversion achieved by using 0.19 g as compared to 0.12 g of Au(DP)/T-S(α) reduced the PO selectivity by about 10% at temperatures above 443 K. A similar effect occurred upon increasing the charge of (Au : Ti, 200 : 1)/S from 0.30 to 0.61 g. Again, a selectivity increase in ethanal compensated for the loss of PO at temperatures above 443 K while almost no changes in selectivity were observed at 413 K and below. There are two important conclusions to be drawn. The higher sensitivity of the selective PO catalysts to oxidative cracking of PO at higher temperatures reaffirms the presence of a low-temperature window for optimal PO yield. On the other hand, at lower temperatures, the Au(DP)/T-S(α) and (Au : Ti, 200 : 1)/S catalysts show less degradation of PO selectivity with decreasing WHSV, indicating higher resistance to sequential PO oxidation as compared to Au(DP)/A and (Au)/P25.

The propylene and oxygen TOFs were independent of WHSV, despite different propylene conversions, supporting the conclusion that the source of the increased ethanal formation was further PO reaction. Despite the decrease in PO selectivity for Au(DP)/T-S(α) and Au(DP)/A, small increases in the PO yield were still observed due to the increased propylene conversion. These results suggest that special attention must be paid to compare propylene oxidation selectivities over Au/TiO_2 catalysts at very similar conversions, as small changes in WHSV have large effects on the observed kinetics.

3.4. H_2/D_2 Kinetic Isotope Effect

Substitution of D_2 for H_2 during propylene oxidation over Au(DP)/T-S(α) and (Au : Ti, 200 : 1)/S produced noticeable kinetic effects as reported in Table 7 at 413 K. Clearly, the PO TOF was suppressed upon D_2 substitution. In fact, the rates for water and all products except acrolein were reduced, resulting in a lower total conversion of both oxygen and propylene. This kinetic isotope effect (KIE) indicated that hydrogen from H_2 was bonded to an intermediate involved in the rate-limiting step for the formation of most products. The TOF suppression of the oxygenates and CO_2, except acrolein, suggests that PO may be a source of these products through a consecutive reaction. The lack of a decrease in rate for acrolein upon D_2 substitution shows that bonds to hydrogen from molecular H_2 are not involved in the rate-limiting step for this product. Abstraction of the allylic hydrogen on the surface of larger bulk gold particles is a likely first step in that pathway (6). An investigation of the KIE over the entire temperature range of interest is published elsewhere (40).

3.5. H_2 Concentration Effects

The effect of H_2 partial pressure on the product distribution at 473 K was tested at six points in the range of 1.9 to 58.4 vol% using Au(DP)/T-S(β). The determined reaction orders and selectivity changes are presented in Table 8.

Only acrolein had a negative reaction order in H_2, suggesting either that it was consumed at a rate greater than its formation with increasing H_2 partial pressure, or that H_2 competed for acrolein formation sites. A reaction order between 0 and 1 for the other species suggested that some form of chemisorbed H_2 or H adatom was necessary for reaction. In our work at 373 K, the PO reaction order in H_2 was 0.5 for conditions of near 100% PO selectivity. This H_2 reaction order obtained for PO formation agreed well with a value of 0.4 extracted indirectly from two points in Fig. 4 of Ref. (25) at 350 K for conditions of 10% O_2, 10% C_3H_6,

TABLE 7

Effect of D_2 Substitution on Product Formation Rate and Selectivity for the Au(DP)/T-S(α) and (Au : Ti, 200 : 1)/S Catalysts at 413 K: Activity Test Conducted Using 0.19 g and 0.30 g of DP and (200 : 1), Respectively

	Au(DP)/T-S(α)				(Au : Ti, 200 : 1)/S			
	with H_2		with D_2		with H_2		with D_2	
Species	TOF ($\times 10^3$ s^{-1})	Sel. (%)	TOF ($\times 10^3$ s^{-1})	Sel. (%)	TOF ($\times 10^3$ s^{-1})	Sel. (%)	TOF ($\times 10^3$ s^{-1})	Sel. (%)
Propylene	13.0	0.47[a]	8.9	0.32[a]	5.8	0.13[a]	4.9	0.11[a]
Oxygen	9.0	0.47[b]	5.9	0.31[b]	3.5	0.12[b]	2.9	0.10[b]
Deuterium			62.3	2.60[c]			50.0	1.32[c]
Ethanal	1.1	5.6	0.5	3.6	0.4	4.5	0.07	1.0
PO	12.0	89.3	8.2	91.5	5.0	85.0	4.4	88.7
Acetone	0.09	0.7	0.06	0.7	0.2	3.3	0.1	2.4
Propanal	0.05	0.3	0.02	0.3	0.2	4.4	.09	1.8
Acrolein	0.02	0.2	0.03	.3	0.1	2.3	0.2	3.9
CO_2	1.6	4.0	1.0	3.7	0.4	2.4	0.3	2.2

Note. Reaction conditions were $C_3H_6/O_2/D_2/He = 10/10/10/70\%$ at 35 STP cc min^{-1}.
[a] Conversion of propylene in %.
[b] Conversion of oxygen in %.
[c] Approximate conversion of deuterium in %.

and variable H_2 concentration. The change in reaction order with temperature may represent differences in surface coverage of an active species involving H_2.

Changes in the H_2 partial pressure had a strong effect on the product selectivity above 10 vol% H_2. Table 8 shows that the selectivity to PO, propanal, and CO_2 only significantly changed with H_2 concentration above 10 vol%. While the PO selectivity decreased by 14% over the H_2 concentration range tested, the ethanal and CO_2 selectivity increased from 9.3–22.3% and CO_2 selectivity increased 8.4–11.9%, respectively. Once again there appeared to be a concomitant tradeoff in selectivity between PO and the oxidative cracking product, ethanal. Propane was formed at large H_2 partial pressures. Propylene conversion was increased at a slower rate as compared to oxygen conversion with higher H_2 concentrations resulting from an enhanced rate of water formation.

Decreased H_2 efficiency at higher H_2 partial pressure is a problem, since poor H_2 efficiencies are already a disadvantage of these catalysts (28). We could not directly determine H_2 efficiency in our experimental setup, but D_2 was somewhat more linear in our GC analysis. At 413 K, the D_2 efficiency for Au(DP)/T-S(α), (Au : Ti, 200 : 1)/S, and Au(DP)/A was approximately 12%, 8%, and 1% respectively. As previously observed, efficiency decreased with increasing temperature as oyxgen conversion rose more quickly than propylene conversion (25, 28). The H_2 efficiency was most likely lower for these catalysts since D_2 appeared to suppress the water formation rate. D_2 TOF and conversion data are presented in Table 7 for comparison with the stated qualifications.

TABLE 8

Effects of H_2 Partial Pressure on Product Selectivity over 0.05 g of DP Au(DP)/T-S(β) at 473 K: Reaction Orders Presented Assume a Power Law Model is Applicable

Species	Reaction order at 473 K	Selectivity at 1.9 vol% H_2 (%)	Selectivity at at 10 vol% H_2 (%)	Selectivity at at 58.4 vol% H_2 (%)
Propylene	0.45	0.6	1.2	2.6
Oxygen	0.50	0.7	1.6	4.0
Ethanal	0.71	9.3	12.7	22.3
PO	0.39	74.0	73.7	60.1
Acetone	0.38	3.4	2.8	2.7
Propanal	0.60	1.5	1.4	2.3
Acrolein	−0.25	3.4	1.1	0.3
CO_2	0.56	8.4	8.3	11.9
Propane				0.3

Note. Reaction conditions were $C_3H_6/O_2/H_2/He = 10/10/x/(100\text{-}x)\%$ at 40 STP cc min^{-1}.

3.6. PO and Acrolein Oxidation

To assess reactivity of PO to other products and the possibility of an independent pathway to acrolein, we studied the direct oxidation of these products. PO oxidation experiments were performed over Au(DP)/T-S(α), the pure T-S support material, and Au powder. Acrolein oxidation was performed only over Au(DP)/T-S(α). The product TOFs are shown in Table 9. The TOF over the T-S support material was calculated assuming that it had the same number of active sites per gram as the Au(DP)/T-S(α) catalyst. The nominal PO concentration produced over the DP catalyst surface at the normal propylene oxidation conditions was

TABLE 9

PO and Acrolein Oxidation over 0.13 g of Au(DP)/T-S(α), 0.15 g of T-S Support, and 0.61 g of High-Purity Au Powder (Au) at 413 K

	Experiment			
	Acrolein oxd.	PO oxd.		
Species	Au(DP)/T-S(α) TOF ($\times 10^3$ s^{-1})	Au(DP)/T-S(α) TOF ($\times 10^3$ s^{-1})	T-S TOF ($\times 10^3$ s^{-1})	Au TOF ($\times 10^3$ s^{-1})
Ethanal	0.6	1.0		0.1
PO		—	—	—
Acetone	0.03	0.1	2.0	0.02
Propanal	0.01	0.05	0.02	0.06
Acrolein	—			
CO_2	5.0	3.0	0.5	0.3
PO/acrolein feed conc. (vol%)	0.1	0.6	0.6	0.6

Note. Reaction conditions were $O_2/H_2/He = 10/10/80\%$ at 35 STP cc min^{-1}, with the saturated feed concentration of hydrocarbon given below. For comparision, the T-S support TOF is calculated assuming it has the same number of active Au sites as Au(DP)/T-S(α).

around 0.1% at 413 K, and for acrolein it was much lower. As a consequence, the surface coverages of PO or acrolein during the product oxidation experiments were substantially different than those during the actual propylene oxidation experiment. This must be considered when interpreting the results.

Acrolein oxidation at 413 K over Au(DP)/T-S(α) with a feed concentration of 0.1 vol% resulted in small amounts of hydrogenation products, propanal and acetone, but the majority of the acrolein was oxidatively cracked to ethanal and CO_2. As the partial pressure of acrolein was increased at the same concentrations of H_2 and O_2, ethanal selectivity increased relative to that of CO_2. This may indicate that for total combustion, multiple sites are required and acrolein competes for those sites. At 473 K, however, the only product observed was CO_2. During the acrolein experiment, PO was not formed.

PO oxidation over Au(DP)/T-S(α) indicated that some isomerization to acetone and propanal occurred, but as in the case of acrolein, the largest selectivity was to ethanal and CO_2. Increasingly more oxidative cracking versus isomerization products were formed as temperatures approached 473 K. In contrast, a high selectivity to acetone was observed over the T-S support. Raising the temperature to 473 K resulted in 100% PO conversion with acetone selectivities above 90%. At all temperatures, very little ethanal and CO_2 was formed in the absence of gold. PO experiments over pure gold powder showed primarily combustion activity, suggesting that the gold–titania interface was responsible not only for PO formation, but also for PO oxidative cracking to ethanal and CO_2.

4. DISCUSSION

While gold powder and TiO_2 alone did not show substantial reactivity toward propylene oxidation under the reaction conditions employed in this paper, the complex synergy created through intimate gold–titania contacting appeared essential for the production of partial oxidation capability. Almost all preparation methods that produced Au particles above 4 nm in size showed some PO formation in a mixture of propylene, O_2, and H_2, but gold–titania contacting alone did not ensure high PO activity/selectivity. Variations of 4 orders of magnitude for PO TOF and selectivities from 0–100% were achieved depending on the catalyst preparation method, the titanium phase and/or local concentration at the active site, and the temperature. There is clearly an optimal level and mode of gold–titania contacting in order to achieve propylene epoxidation.

The effects of the catalyst preparation method are clearly seen in our sequential attempts to increase the strength (intimacy) of the gold–titania contacting. PO activity was created by impregnating an inactive gold powder with TiO_2 or by the leaching of an $AuTi_3$ alloy. Activity to oxygenates over these modified Au powders was low, however, due to the small number of gold–titania active contact sites, a limitation which we attempted to overcome by dispersing fine gold particles onto titania supports. This resulted in catalysts that exhibit higher PO TOFs as compared to modified Au powders, but not necessarily higher PO selectivity. The activity of (Au)/P25 at 473 and 443 K was very similar to that of the most active modified gold powder, 0.5-T/Au, which actually was slightly more selective to partial oxidation products. Apparently just supporting many gold particles with diameters under 10 nm in size on any titania support was not sufficient to provide adequate interface contact synergy for PO formation. The larger surface area of P25, as discussed later, may also play a role. High-temperature treatments, such as that applied to HTC(Au)/P25, appeared to increase contact synergy and gave higher PO selectivities, but at the expense of total propylene conversion. Impregnating anatase with a gold salt, Au(I)/A, provided active PO sites despite an apparently large Au particle size, and this activity appeared to be better than that obtained via colloidal deposition methods combined with calcination temperatures around 573 K.

The most effective catalyst preparation methods for high PO activity were found in catalysts in which gold was initially deposited as oxidized species, such as in CP or DP methods. Also, methods in which the gold and titania phases were synthesized at the same time, as in the case of certain DACS bimetallic catalysts, produced materials with higher PO TOFs. Similarly, Au/TiO_2 catalysts prepared from special chloride-free gold organometallic complexes achieve high low-temperature CO oxidation activity (7, 11, 13, 14). Here, DP catalysts proved to be best for producing high PO

activity. When gold is deposited as a nonmetallic chloride-free species during catalyst preparation, there is a better opportunity for forming contacts between the gold and titania phases capable of propylene epoxidation. EXAFS studies of gold DP onto titania supports show that as the pH at synthesis is increased, so is the fraction of Au–Ti bonds relative to Au–Au bonds (41). PO activity most likely increases with the number of Au–Ti, or more likely Au–O–Ti, bonds.

After a gold–titania catalyst has been initially synthesized, the calcination temperature used to "cure" the catalyst can be vital in determining the final activity. This has been definitively shown for low-temperature CO oxidation (14, 15, 17). Both Yuan *et al.* (14) and Tsubota *et al.* (15) have shown that for initially less optimally contacted Au/TiO_2 catalysts, activity can be improved by increasing the calcination temperature. The best preparation methods, however, show optimal calcination temperatures of about 673 K, above which activity is seen to decrease. In this work, high-temperature calcination of (Au)/P25 at 873 K resulted in an increase in PO activity and selectivity, despite sintering and decreased propylene conversion. This is most likely attributed to an increased number of Au–Ti bonds, perhaps through Ti migration, although SMSI states appear to have been discounted for impregnated catalysts (38). The difference in calcination temperature and gold loadings for certain catalysts in this work can complicate comparisons. Non-optimally contacted catalysts in this study could probably show improved selectivity and PO yield with more careful study of calcination effects, as has been overserved for CO oxidation (14). These effects for already more optimally contacted catalysts (such as DP) are more complicated (14), and have not been thoroughly studied for propylene epoxidation.

While the preparation method and calcination temperature play a role in determining the PO activity and selectivity, another very important factor appeared to be the TiO_2 phase and/or local concentration in contact with the gold. Table 2 shows that increased TiO_2 loadings over modified Au powders resulted in nonselective reactions to non-PO partial oxygenates and CO_2. (Au : Ti, 4 : 1)/S, which TEM showed to be largely titania-encapsulated gold particles, had the largest selectivity to oxidative cracking products within the subset of bimetallic cluster catalysts. In contrast, DACS bimetallic catalyst with higher Au : Ti ratios appeared to be capable of maintaining better PO selectivity by minimizing ethanal formation over the experimental temperature range. When gold is deposited on titania, the type of titania support may influence the wetting and shape of the gold particles, thereby altering the type and number of interfacial contacts. The same DP method for depositing gold on three different supports—P25, anatase, and titania-modified-silica—produced three catalysts of vastly different PO activity and selectivity at temperatures higher than 373 K. There was evidence that any long-range TiO_2 phase structure was detrimental to PO activity and selectivity at higher temperatures; rutile phases were the worst, anatase was slightly better, and the titania-modified-silica was best. Well-dispersed DP gold particles on TS-1 have been found to be very active for propylene epoxidation (28), with TS-1 representing perhaps the highest achievable level of Ti dispersion.

Attempts to increase the propylene conversion by increasing the temperature or decreasing the WHSV result in decreased PO selectivity regardless of catalyst preparation or titanium support phase. PO is known to strongly interact with TiO_2, perhaps limiting the epoxidation reaction through two means: PO oligomerization on the catalyst surface or product rate inhibition (28). Our PO oxidation studies also supported the conclusion that PO strongly interacted with the catalyst surface. Over T-S in the presence of H_2, PO isomerized, forming mostly acetone at 413 K with minor amounts of propanal and CO_2. Without H_2, reaction was only observed at 473 K, forming mostly acetone with some propanal. A difference was observed when PO oxidation was performed over Au(DP)/T-S, where the selectivity was dominated by ethanal and CO_2. These results suggest sequential reaction of PO to other partial oxygenates and CO_2 depending on the surface chemistry present. Isomerization of PO to acetone occurs over both acidic and basic oxygen sites that coexist on metal oxide materials in the presence of water (42–44). The strength of each acid or base site is dependent on the titania preparation method (45). Propanal is formed on acid sites from PO, but can also be formed hydrogenation of acrolein (46). The acrolein oxidation studies, however, combined with the D_2 KIE, suggest that the acrolein formation pathway is separate, probably occurring at the surface of the gold particles where the allylic hydrogen is preferentially abstracted (6). Despite their presence in the final reaction mixture, acetone, propanal, and acrolein are usually not significant products compared to the PO oxidative cracking products, ethanal and CO_2. PO oxidation and H_2 concentration studies suggested that oxidative cracking to ethanal and CO_2 was H_2-assisted at the gold–titania interface, as the rate to these products was slower in the absence of gold. Perhaps excess Ti adjacent to the active interface results in nonselective oxidation sites. To increase PO yields, PO oligomerization and the oxidative cracking sites must be controlled by optimizing the amount and phase of titania in contact with the gold.

It is interesting to note from the PO oxidation experiments that, despite very similar reaction conditions, the total PO consumption rate over the T-S support was slightly higher than that over the Au(DP)/T-S(α) catalyst. XPS results indicated that the Au(DP)/T-S(α) catalyst surface was covered with a large amount of Na deposited during the DP preparation method. It is possible that absorbed Na altered PO adsorption and isomerization sites, similar to the situation in which K_2O impregnated on P25 has been shown to

completely change the acid–base character of the surface (47).

Mechanistic information from these studies came primarily from D_2 experiments. The observed D_2 kinetic isotope effect on the PO formation rate is strong support for the hydroperoxy mechanism favored in the literature (25, 28), especially considering that H_2 is not stoichiometrically required to form PO from an oxygen atom and propylene. Olivera *et al.* showed that gold is very good compared to other noble metals at stabilizing hydroperoxy radicals (48). In our study, we were unsuccessful in using CO as a reductive source instead of H_2, or N_2O as an oxidizing source instead of O_2, in the temperature range of 373–473 K, further strengthening the argument for a hydroperoxy species. An increase in H_2 partial pressure appeared to increase the formation of this hydroperoxy intermediate, resulting in an increased rate of PO formation.

5. CONCLUSIONS

Propylene oxide (PO) can be formed through gold–titania intimate contacting by a wide variety of preparation techniques yielding Au particles size with diameter greater than 2 nm. The PO TOFs for Au/TiO_2 catalysts exhibited a relatively small spread at 373 K, but varied over 4 orders of magnitude as temperatures approached 473 K. The amount and phase of titania in contact with gold, influencing the number and type of Au–Ti contacts, is important in maximizing PO formation and limiting both oxidative cracking of PO to ethanal and CO_2 and PO isomerization reactions. The best catalysts synthesized in this study were a DP catalyst prepared on titania-modified silica and an Au–Ti bimetallic cluster catalyst produced in the aerosol reactor. A D_2 kinetic isotope effect observed for PO formation supports the idea that a hydroperoxy intermediate is produced from H_2 and O_2 over the catalyst's surface.

While decreasing catalyst activity with time on stream may have been due in part to PO oligomerization, the effect appeared to be less important at higher temperatures. In this study, PO activity was relatively stable at higher temperatures, and on-stream times significantly longer than 6 to 12 h would be necessary to achieve total catalyst deactivation. Despite any problems that PO oligomerization may cause, H_2 partial pressure, WHSV, and PO oxidation studies suggest that while PO isomerization to acetone and propanal occurred over Au/TiO_2, H_2-assisted PO oxidative cracking reactions at higher temperature were the major source of decreasing PO selectivity. The observed maximum in PO TOF between 373 and 473 K is directly correlated to this loss in PO selectivity and may also reflect decreasing intermediate (hydroperoxy) stability. Low temperatures may require control of PO oligomerization to increase yield and maintain activity, but limiting further reaction of PO with the catalyst surface, especially further interaction at or near the active epoxidation site, seems absolutely necessary for sustained PO yields at any temperature. Steps in this direction have been achieved by controlling synthesis procedures, ensuring Au is contacted to a minimal amount of Ti in the correct coordination. These include DACS catalysts with well-dispersed Ti in a gold matrix and using DP Au on TS-1 (28).

ACKNOWLEDGMENTS

The help of Jia Liu was greatly appreciated in the preparation of Au–Ti colloid samples for XPS analysis.

REFERENCES

1. Hammer, B., and Nørskøv, J. K., *Nature* **376**, 238 (1995).
2. Natio, S., and Tanimoto, M., *J. Chem. Soc., Chem. Commun.* 832 (1988).
3. Schwank, J., Galvagno, S., and Parravano, G., *J. Catal.* **63**, 415 (1980).
4. Schwank, J., *Gold Bull.* **16**, 103 (1983).
5. Hutchings, G. J., *Gold Bull.* **29**, 123 (1996).
6. Cant, N. W., and Hall, W. K., *J. Phys. Chem.* **75**, 2914 (1971).
7. Haruta, M., *Catal. Today* **36**, 153 (1997).
8. Tsubota, S., Haruta, M., Kobayshi, T., Ueda, A., and Nakahara, Y., "Preparation of Catalysts V," p. 695. Elsevier, Amsterdam, 1991.
9. Lin, S. D., Bollinger, M. A., and Vannice, M. A., *Catal. Lett.* **17**, 245 (1993).
10. Haruta, M., Tsubota, S., Kobayshi, T., Kageyama, H., Genet, M., and Delmon, B., *J. Catal.* **144**, 175 (1993).
11. Yuan, Y., Asakura, K., Wan, H., Tsai, K., and Iwasawa, Y., *Catal. Lett.* **42**, 15 (1996).
12. Bemwenda, G. R., Tsubota, S., Nakamura, T., and Haruta, M., *Catal. Lett.* **44**, 83 (1997).
13. Yuan, Y., Kozlove, A. P., Asakura, K., Wan, H., Tsai, K., and Iwasawa, Y., *J. Catal.* **170**, 191 (1997).
14. Yuank, Y., Asakura, K., Kozlova, A. P., Wan, H., Tsai, K., and Iwasawa, Y., *J. Catal.* **44**, 333 (1998).
15. Tsubota, S., Nakamura, T., Tanaka, K., and Hartua, M., *Catal. Lett.* **56**, 131 (1998).
16. Grundwalt, J. D., Kiener, C., Wogerbauer, C., and Baiker, A., *J. Catal.* **181**, 223 (1999).
17. Bollinger, M. A., and Vannice, M. A., *Appl. Catal. B* **8**, 417 (1996).
18. Liu, Z. M., and Vannice, M. A., *Catal. Lett* **43**, 51 (1997).
19. Boccuzzi, F., Chiorino, A., Tsubota, S., and Haruta, M., *J. Phys. Chem.* **100**, 175 (1996).
20. Valden, M., Lai, X., and Goodman, D. W., *Science* **281**, 1647 (1998).
21. Su, Y. S., Lee, M. Y., and Lin, S. D., *Catal Lett.* **57**, 49 (1999).
22. Dekers, M. A. P., Lippits, M. J., and Nieuwenhuys, B. E., *Catal. Lett.* **56**, 195 (1998).
23. Grundwalt, J. D., and Baiker, A., *J. Phys. Chem. B* **103**, 1002 (1999).
24. Hayashi, T., Tanaka, K., and Haruta, M., *Am. Chem. Soc., Div. Pet. Chem.* **41**, 71 (1996).
25. Hayashi, T., Tanaka, K., and Haruta, M., *J. Catal.* **178**, 566 (1998).
26. Haruta, M., Uphade, B. S., Tsubota, S., and Miyamoto, A., *Res. Chem. Intermed.* **24**, 329 (1998).
27. Kalvachev, Y. A., Hayashi, T., Tsubota, S., and Haruta, M., *J. Catal.* **186**, 228 (1999).
28. Nijhuis, T. A., Huizinga, B. J., Makkee, M., and Moulijn, J. A., *Ind. Eng. Chem. Res.* **38**, 884 (1999).
29. Chao, L. C., and Andres, R. P., *J. Colloid Interface Sci.* **165**, 290 (1994).
30. Mahoney, W. J., and Andres, R. P., *Mater. Sci. Eng.* **204**, 160 (1995).
31. Castillo, R., Koch, B., Ruiz, P., and Delmon, B., *J. Catal.* **161**, 524 (1996).

32. Heath, J. R., Knobler, C. M., and Leff, D. V., *J. Phys. Chem. B* **101**, 189 (1997).
33. Scofield, J. H., *J. Electron Spectrosc. Relat. Phenom.* **8**, 129 (1976).
34. Tanuma, S., Powell, C. J., and Penn, D. R., *Surf. Interface Anal.* **11**, 577 (1988).
35. Viljoen, P. E., and Roux, J. P., *Vacuum* **41**, 1746 (1990).
36. Kim, K. S., and Winograd, N., *Chem. Phys. Lett.* **30**, 91 (1971).
37. Fogler, H. S., "Elements of Chemical Reaction Engineering," 2nd ed. Prentice Hall, Englewood Cliffs, NJ, 1992.
38. Shastri, A. G., Datye, A. K., and Schwank, J., *J. Catal.* **87**, 265 (1984).
39. Wagner, F. E., Galvagno, S., Milone, C., Visco, A. M., Stievano, L., and Calogero, S., *J. Chem. Soc., Faraday Trans.* **93**, 3403 (1997).
40. Stangland, E. E., Stavens, K. B., Andres, R. P., and Delgass, W. N., "Proceedings of the 12the International Congress on Catalysis, Granada, Spain, 2000," Stud. Surf. Sci. Catal., accepted.
41. Kageyama, H., Tsubota, S., Kadono, K., Fukumi, K., Akai, T., Kamijo, N., and Haruta, M., *J. Phys. IV, Colloq. C2* **7**, 935 (1997).
42. Bartók, M., Notheisz, F., and Kiss, J. T., *J. Catal.* **68**, 249 (1981).
43. Coq, B., Figueras, F., Geneste, P., Moreau, C., Moreau, P., and Warawdekar, M., *J. Mol. Catal.* **78**, 935 (1993).
44. Salmón, M., Pérez-Luna, M., Lopéz-Franco, C., Hernández, E., Alvarez-Ramírez, R. A., López-Ortega, A., and Domínguez, J. M., *J. Mol. Catal. A* **122**, 169 (1997).
45. Kung, H. H., "Transition Metal Oxides: Surface Chemistry and Catalysis," Studs. Surf. Sci. Catal. 45. Elsevier, Amsterdam/New York, 1989.
46. Marinelli, T. B. L. W., and Ponec, V., *J. Catal.* **156**, 51 (1995).
47. Busca, G., and Ramis, G., *Appl. Surf. Sci.* **27**, 115 (1986).
48. Olivera, P. P., Patrito, E. M., and Sellers, H., *Surf. Sci.* **313**, 25 (1994).